Supplemental material

De La Rosa et al., https://doi.org/10.1085/jgp.201711822

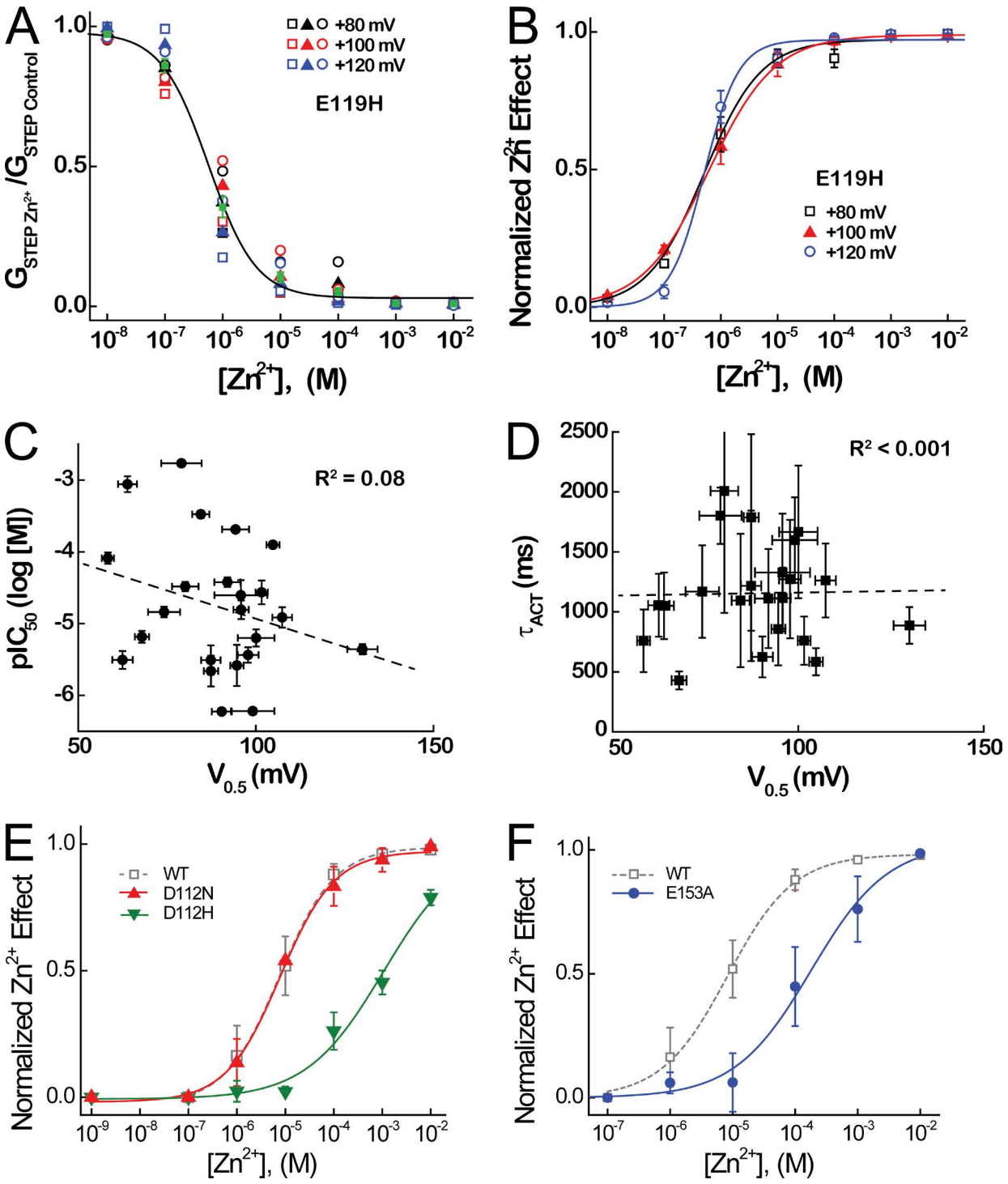

Figure S1. **Effects of P_{OPEN} and mutation on apparent Zn^{2+} potency. (A)** To determine the effect of Zn^{2+} at similar P_{OPEN} in mutants with shifted P_{OPEN}-voltage relations, we measured Zn^{2+} concentration responses at different step potentials (Table 1). Data represent G_{STEP} measured at the indicated $[Zn^{2+}]$ normalized to its respective maximum in the absence of Zn^{2+} at V_{STEP} = +80 mV, P_{OPEN} ~ 0.8 (black symbols), V_{STEP} = +100 mV, P_{OPEN} ~ 0.55 (red symbols), and V_{STEP} = +120 mV, P_{OPEN} ~ 0.3 (blue symbols) in different cells; each symbol shape represents data from an individual cell. Mean (± SEM) normalized G_{STEP} values for the three cells shown here is represented by filled green squares, and the black line represents a logistic fit of the data ($G_{STEPmax}$ = 0.98, $G_{STEPmin}$ = 0.03, IC_{50} = 0.57 µM, P = 1.06). **(B)** Mean (± SEM, *n* = 3 cells) responses at each voltage (data from A: +80 mV, open black squares; +100 mV, filled red triangles; +120 mV, open blue circles) are plotted as normalized Zn^{2+} effect. Lines represent fits of the data to a Hill function (+80 mV: black line, IC_{50} = 0.51 µM, n_H = 0.9; +100 mV: red line, IC_{50} = 0.61 µM, n_H = 0.7; +120 mV: blue line, IC_{50} = 0.51 µM, n_H = 1.4). **(C)** Mean (± SEM) $V_{0.5}$ and Zn^{2+} pIC_{50} values for each mutant listed in Table 1 are plotted. The dashed line represents a linear fit of the data to a straight line of the form pIC_{50} = −3.3 + −0.01·($V_{0.5}$). **(D)** Mean (± SEM) τ_{ACT} and $V_{0.5}$ values for each mutant listed in Table 1 are plotted. The dashed line represents a linear fit of the data to a straight line of the form pIC_{50} = 1,095 + 0.68·($V_{0.5}$). **(E and F)** Zn^{2+} potency in E (D112N and D112H) or F (E153A) is compared with WT Hv1. Lines represent Hill fits to the data (D112N: IC_{50} = 9.5 µM; n_H = 0.76; D112H: IC_{50} = 1139.3 µM; n_H = 0.56; E153A: IC_{50} = 241.2 µM; n_H = 0.87; see Table 1).

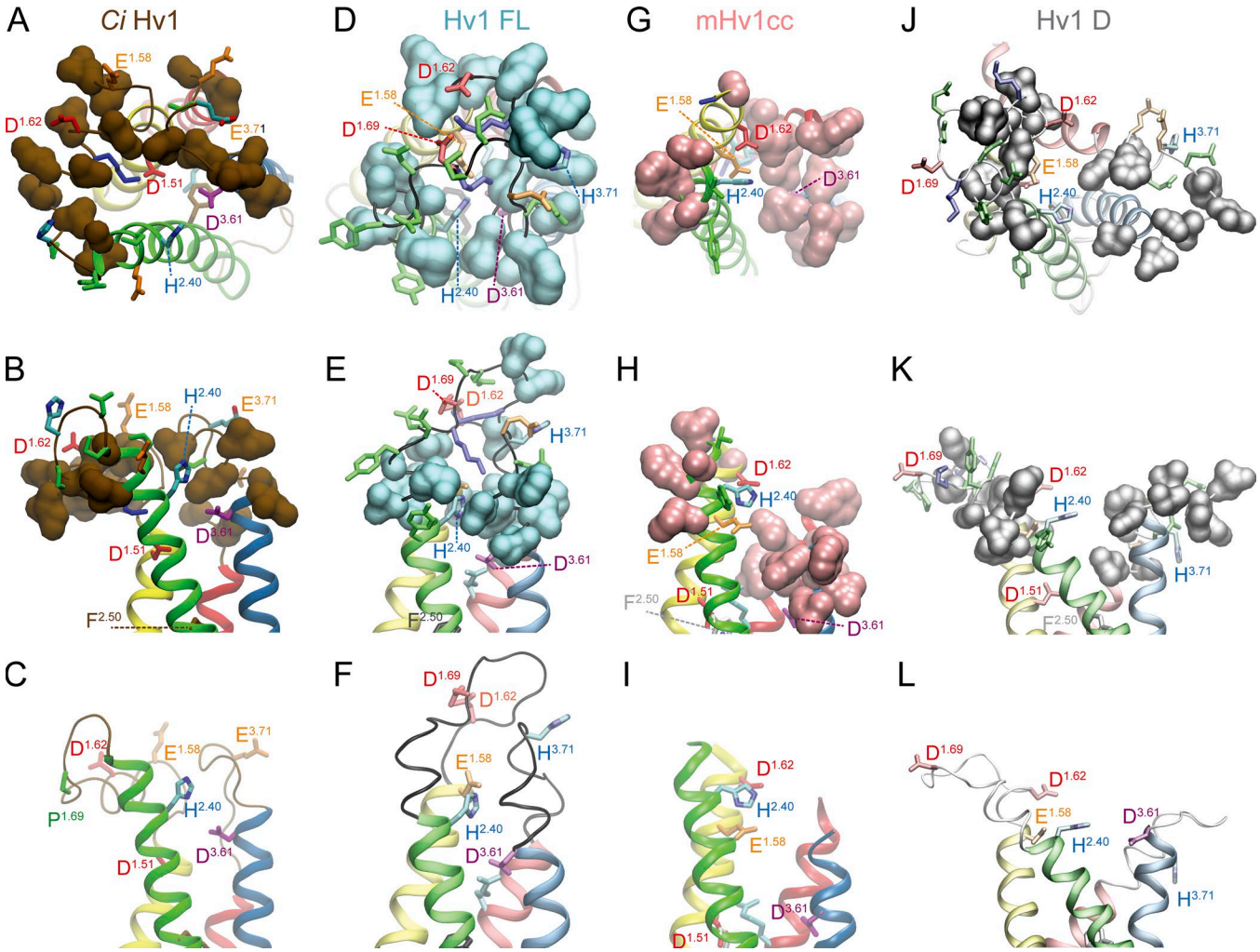

Figure S2. **Comparison of extracellular faces in Hv1 model and x-ray structures.** Side chains located at or near the extracellular face of Hv1 model and x-ray structures are illustrated in representations of *Ci* Hv1 (A–C), Hv1 FL (D–F), mHv1cc x-ray (PDB accession no. 3WKV; G–I), and Hv1 D (J–L) model structures. Ionizable side chains are shown in colored licorice (Asp: red; Glu: orange; Arg and Lys; blue; His: cyan/blue), polar neutral side chains (Asn, Gln, and Tyr) are shown in green licorice, and hydrophobic side chains (including $L^{1.59}$, $I^{1.60}$, $L^{1.61}$, $L^{1.63}$, $I^{1.64}$, $I^{1.65}$, $I^{3.62}$, $V^{3.63}$, $L^{3.64}$, $V^{3.65}$, $F^{3.66}$, $F^{4.37}$, $A^{4.39}$, and $L^{4.40}$ in Hv1 FL and Hv1 D, and their equivalents in *Ci* Hv1 and mHv1cc) are shown by colored (*Ci* Hv1, brown; Hv1 FL, cyan; mHv1cc, pink; Hv1 D, gray) space-filling surface representations in the top two panels.

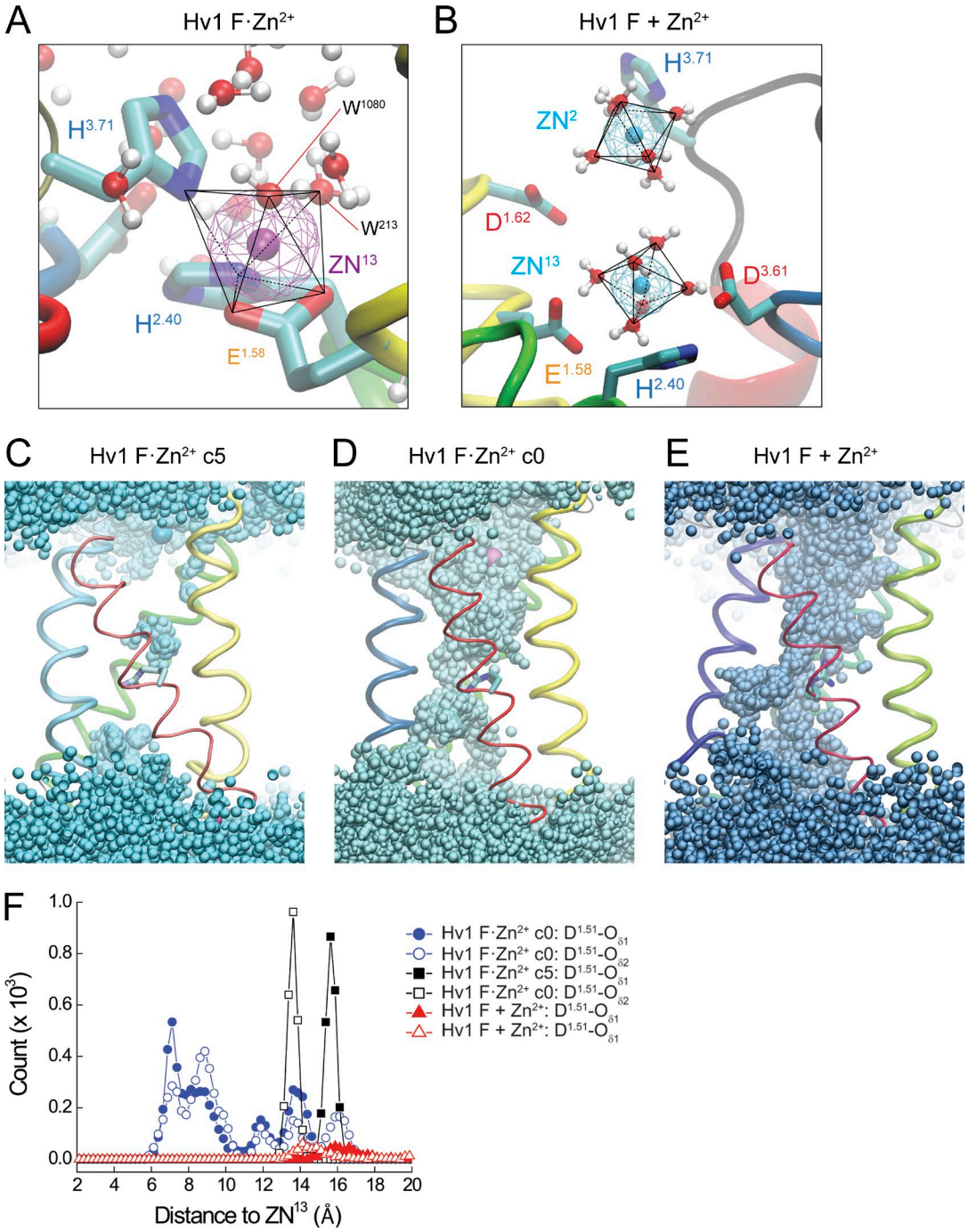

Figure S3. **Zn^{2+} coordination and hydration in Hv1 F·Zn^{2+} and Hv1 F + Zn^{2+} MD simulations.** Related to Figs. 1 and 5. **(A and B)** Snapshots taken from Hv1 F·Zn^{2+} (A: t = 110 ns; Fig. 5, H and I) and Hv1 F + Zn^{2+} (B: t = 1.6 ns; Fig. 5, F and G) MD simulations show octahedral coordination of Zn^{2+} ions (magenta or cyan wireframe representations) by protein and water atoms (black lines). In A, water molecules (solid red and white CPK representations) shown are within 8 Å of ZN^{13}. In B, waters that are not in the first solvation shells of either ZN^{2} or ZN^{13} are omitted for clarity (but see Fig. S8). Black lines in A and B (solid, foreground; dashed, background) illustrate octahedral Zn^{2+} coordination geometries (A: H140/$H^{2.40}$-$N_{\delta1}$, H193/$H^{3.71}$-$N_{\delta1}$, E119/$E^{1.58}$-$O_{\varepsilon1}$, E119/$E^{1.58}$-$O_{\varepsilon2}$, W^{213}-O_1, and W^{1080}-O_1; B: water oxygen atoms). Mean distances between ZN^{2} or ZN^{13} and first-shell water oxygen atoms are 2.100 ± 0.004 Å or 2.100 ± 0.002 Å, respectively (first 10 ns of the Hv1 F + Zn^{2+} MD simulation); the mean distance between ZN^{2} and ZN^{13} is 6.88 ± 0.68 Å (t = 10–30 ns in Hv1 F + Zn^{2+} MD simulation). **(C–E)** Water occupancy in Hv1 F·Zn^{2+} before (C; Hv1 F·Zn^{2+} c5) and after (D; Hv1 F·Zn^{2+} c0) removal of 5 kcal/mol/Å harmonic constraints between ZN^{13}-$H^{2.40}$-$N_{\delta1}$ and ZN^{13}-$H^{3.71}$-$N_{\delta1}$ bonds and in the Hv1 F + Zn^{2+} system (E) is shown for every 10th frame during a selected 10-ns segment of each MD simulation. Backbone structures (ribbons), as viewed from within the plane of the membrane, are colored as described previously. The R1 side chain is shown in licorice representation, water molecules are shown as cyan (C), aqua (D), or blue (E) beads, and ZN^{13} is represented as a solid light blue (C) or magenta (D and E) sphere. Zn^{2+} ions are not visible in E but are located within the hydrated extracellular vestibule, as shown in Fig. 5 (C and D). **(F)** Distance histograms for ZN^{13} to $D^{1.51}$-$O_{\delta1}$ (filled symbols) or $D^{1.51}$-$O_{\delta2}$ (open symbols) calculated during 120 ns Hv1 F·Zn^{2+} c0 (blue circles), 50 ns Hv1 F·Zn^{2+} c5 (black squares), and 120 ns Hv1 F + Zn^{2+} (red triangles) MD trajectories. Note that the first solvation shell interactions (peak at ∼2.1 Å) between Zn^{2+} and $D^{1.51}$ terminal oxygen atoms are not observed in these simulations.

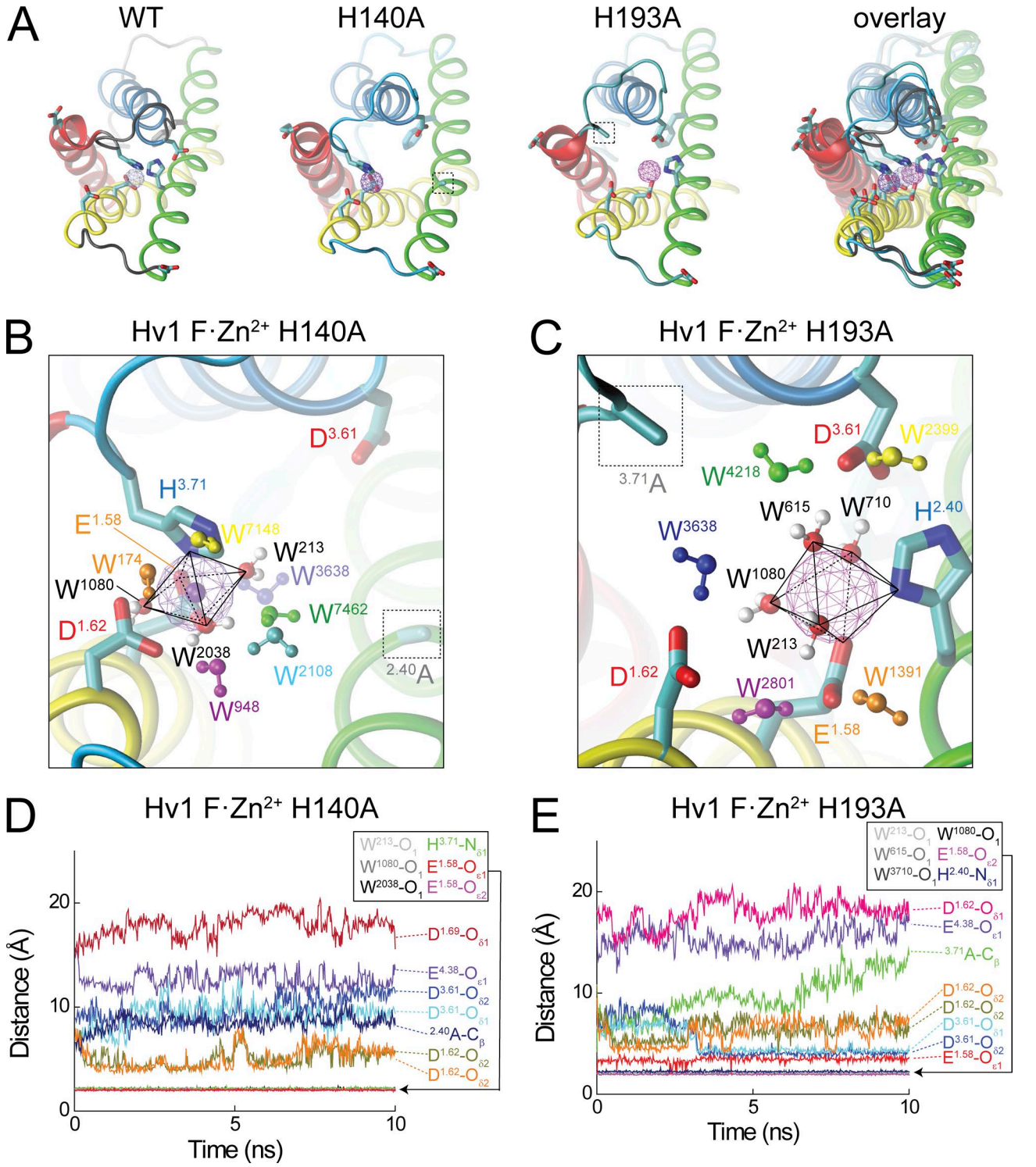

Figure S4. **Effect of H140A and H193A mutations on Hv1 F structure.** Related to Figs. 1, 5, and 6. **(A)** Hv1 F·Zn^{2+} H140A (middle left) and Hv1 F·Zn^{2+} H193A (middle right) mutant model structures are compared with WT Hv1 F·Zn^{2+} (left), as illustrated by the overlay (right). MD simulations of mutant models are conducted with 5 kcal/mol/Å harmonic constraints applied (ZN^{13} to $H^{3.71}$-$N_{\delta1}$ in Hv1 F·Zn^{2+} H140A and ZN^{13} to $H^{2.40}$-$N_{\delta1}$ in Hv1 F·Zn^{2+} H193A). **(B and C)** Magnified extracellular views of Zn^{2+} ion (ZN^{13}, magenta wireframes) coordination in snapshots selected from Hv1 F·Zn^{2+} H193A (B) and Hv1 F·Zn^{2+} H193A (C) MD simulation trajectories (t = 10 ns). The positions of mutated residue side chains are highlighted by dashed boxes. **(D and E)** Distances between ZN^{13} and selected atoms in Hv1 F $H^{2.40}$A·Zn^{2+} (D) and Hv1 F $H^{3.71}$A·Zn^{2+} (E) over 10 ns of MD simulation time are shown by colored lines. Atoms that participate in first-shell coordination of ZN^{13} are enclosed by black boxes.

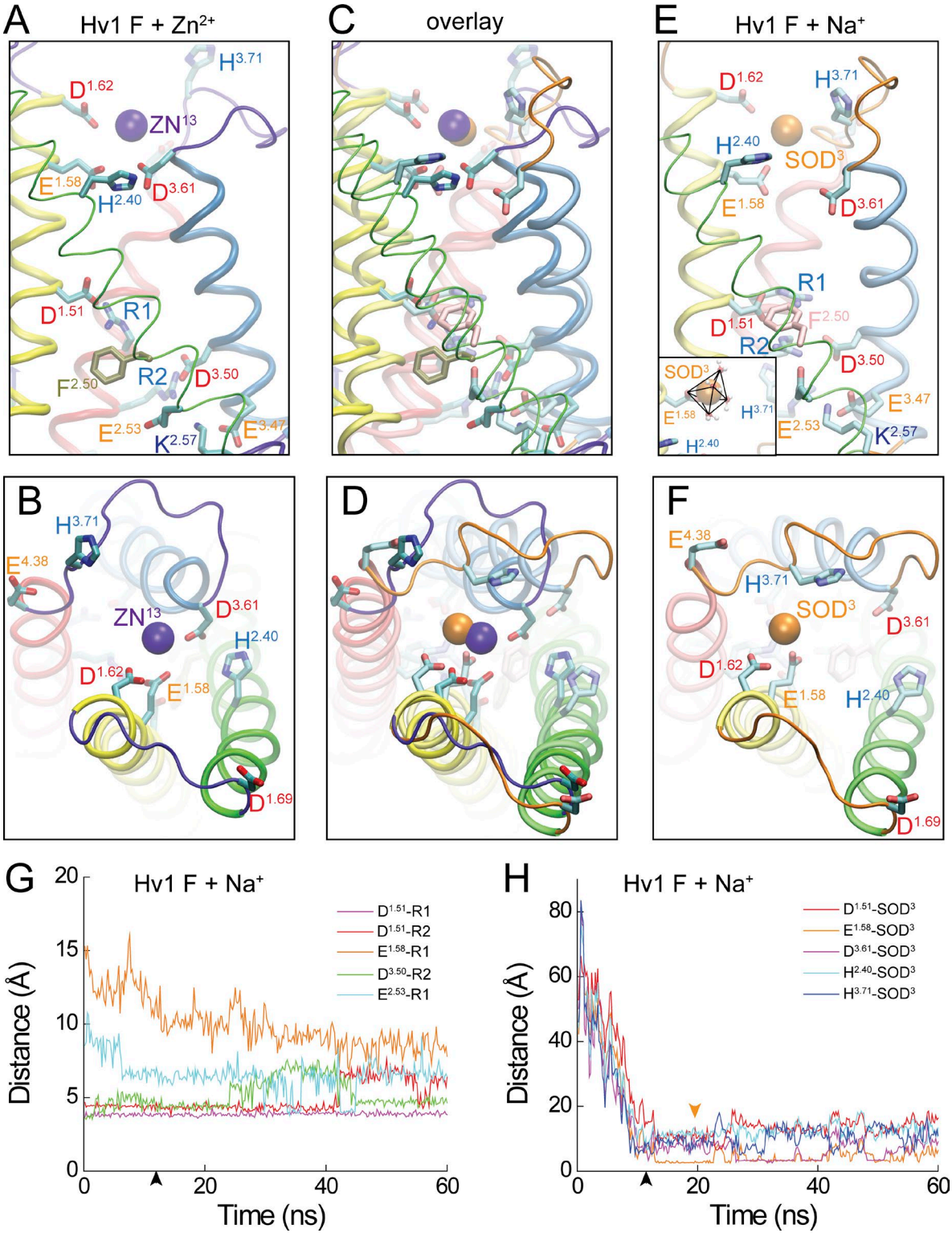

Figure S5. **Comparison of Hv1 F MD simulations conducted in the presence of Na^+ and Zn^{2+}.** Related to Figs. 1, 5, and 6. **(A–F)** Snapshots taken after 12.5 ns (black arrowheads in G and H) of MD simulation time from Hv1 F + Na^+ (E and F) or Hv1 F + Zn^{2+} (A and B) systems (snapshot taken at black arrowhead in Fig. 5 E). Hv1 F + Na^+ and Hv1 F + Zn^{2+} snapshots are overlain in C and D. Model structures are viewed side-on in A, C, and E and from the extracellular side of the membrane in B, D, and F. Backbone structures of transmembrane helices are colored as in previous figures, and loops are colored either violet (Hv1 F + Zn^{2+}) or orange (Hv1 F + Na^+). Side chains are shown in colored licorice as in previous figures; ZN^{13} (Hv1 F + Zn^{2+}) and SOD^3 (Hv1 F + Na^+) are shown as violet or orange spheres, respectively. **(E)** Inset: Na^+ coordination by waters and carboxylate oxygen atoms from $E^{1.58}$ at t = 20 ns (orange arrowhead in H) in the Hv1 F + Na^+ system. **(G)** Distances between terminal carbon atoms in selected side chains during MD simulation of the Hv1 F + Na^+ system are shown as colored lines. **(H)** Distances between terminal carbon atoms in selected side chains and SOD^3 during MD simulation of the Hv1 F + Na^+ system are shown as colored lines.

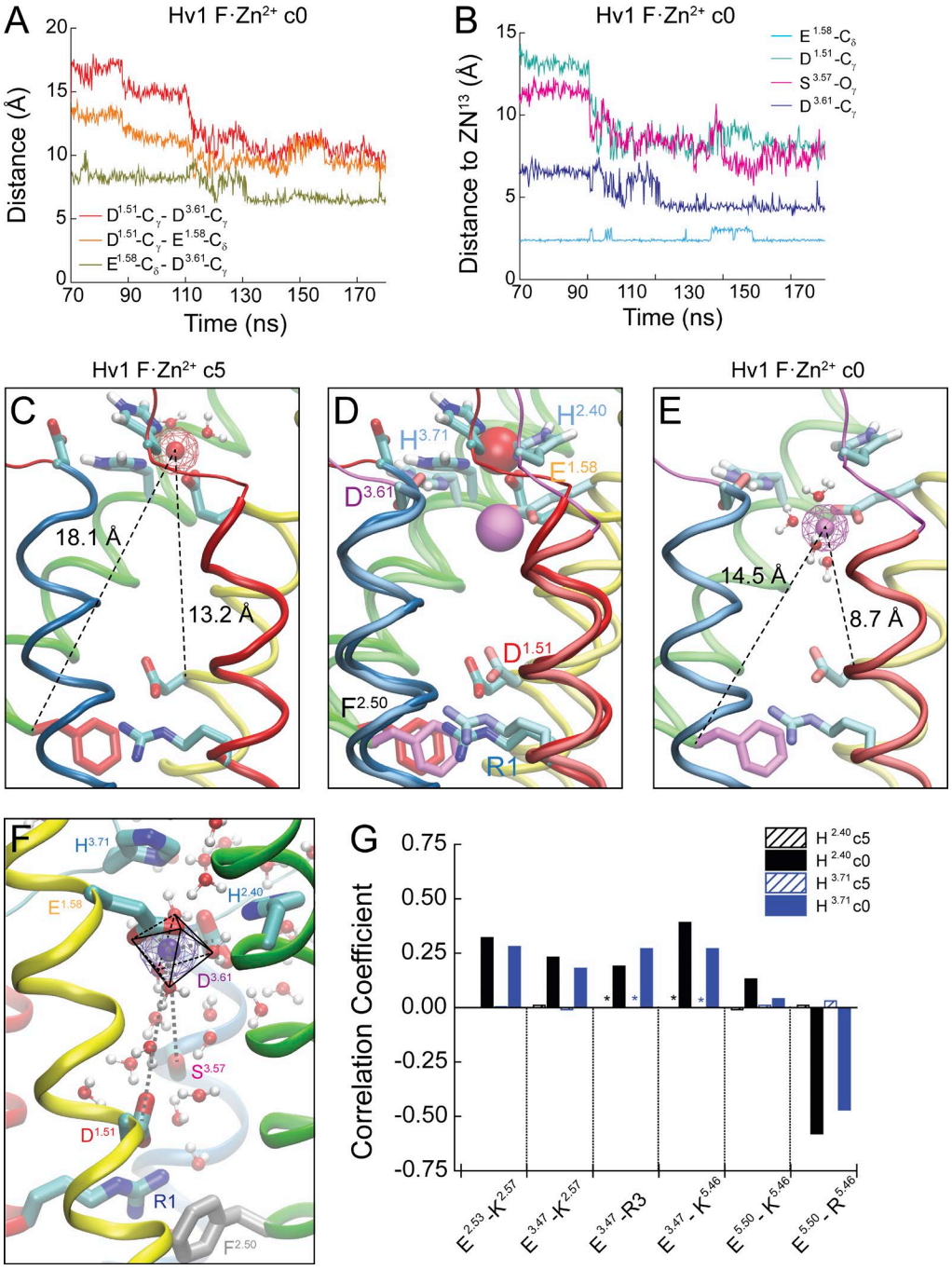

Figure S6. **Zn^{2+} coordination in Hv1 F·Zn^{2+} c0 and Hv1 F·Zn^{2+} c5 MD simulations.** Related to Figs. 5 and 6. **(A and B)** Distances measured between terminal carbon atoms of side chains involved in salt bridges (A) or between ZN^{13} and selected side-chain atoms (B) are shown in function of Hv1 F·Zn^{2+} c0 MD trajectory time. Lines in A represent $D^{1.51}$-C_γ to $D^{3.61}$-C_γ, $D^{1.51}$-C_γ to $E^{1.58}$-C_δ, and $E^{1.58}$-C_δ to $D^{3.61}$-C_γ distances; lines in B represent distances between ZN^{13} and $E^{1.58}$-C_δ, $D^{1.51}$-C_γ, and $S^{3.51}$-C_γ distances. Mean distances between ZN^{13} and the indicated atoms over the final 50 ns of Hv1 F·Zn^{2+} c0 MD simulation time are as follows: $E^{1.58}$-C_δ, d = 2.5 ± 0.3 Å; $D^{1.51}$-C_γ, d = 8.3 ± 0.6 Å; $S^{3.57}$-O_γ, d = 7.9 ± 0.8 Å; and $D^{3.61}$-C_γ, d = 4.7 ± 0.7 Å. **(C–E)** Magnified side views of the extracellular vestibule are shown in snapshots taken from the Hv1 F·Zn^{2+} c0 MD stimulation before (C, t = 90 ns) and after (E, t = 130 ns) dissociation of Zn^{2+} from $H^{2.40}$ and $H^{3.71}$ (Fig. 5, H and I). D shows an overlay of the snapshots depicted in C and E and represented side chains are labeled. ZN^{13} is represented by colored wireframe (C and E) or solid (D) spheres. Distances between ZN^{13} and $F^{2.50}$-C_α or $D^{1.51}$-C_α atoms in the represented snapshots are indicated by dashed black lines and labels. **(F)** The final snapshot of the Hv1 F·Zn^{2+} c0 MD simulation (t = 180 ns) shows octahedral coordination of ZN^{13} (purple sphere surrounded by wireframe) by first solvation shell interactions with $E^{1.58}$-$O_{\varepsilon1}$, $E^{1.58}$-$O_{\varepsilon2}$ and four water oxygen atoms, as indicated by solid and dashed black lines (Figs. 5 I and S3). Mean distances between ZN^{13} and selected atoms over the last 50 ns (t = 130–180 ns) of the Hv1 F·Zn^{2+} c0 MD simulation are shown by dashed gray lines ($D^{1.51}$-C_γ, 8.3 ± 0.6 Å; $E^{1.58}$-C_δ, 2.5 ± 0.3 Å; $S^{3.57}$-O_γ, 7.9 ± 0.8 Å; $D^{3.61}$-C_γ, 4.7 ± 0.7 Å). Not depicted is the mean distance between D112/$D^{1.51}$-C_γ and D185/$D^{3.61}$-C_γ over the final 50 ns of MD simulation time (10.6 ± 0.7 Å). **(G)** PCCs are calculated for changes in the distances of the indicated salt bridges and Zn^{2+}-$N_{\delta1}$ interactions during Hv1 F·Zn^{2+} c5 (ZN^{13} and $H^{2.40}$-$N_{\delta1}$, hashed black columns; ZN^{13} and $H^{3.71}$-$N_{\delta1}$, hashed blue columns) and Hv1 F·Zn^{2+} c0 (ZN^{13} and $H^{2.40}$-$N_{\delta1}$, filled black columns; ZN^{13} and $H^{3.71}$-$N_{\delta1}$, filled blue columns) MD trajectories. Asterisks indicate that an H-bond between the indicated residues is not formed during the indicated MD trajectory. See Table 3 and Fig. 6 G.

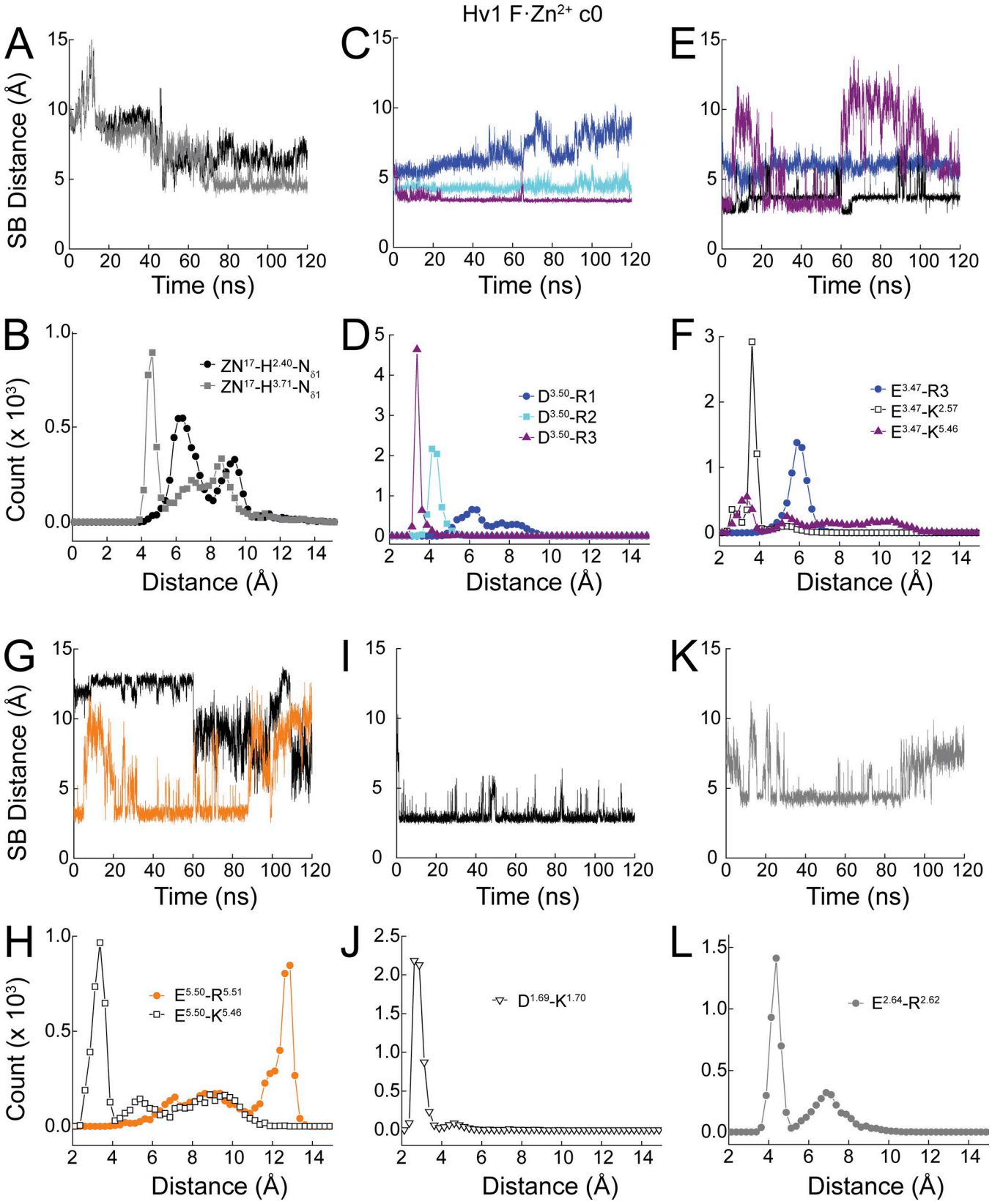

Figure S7. **Salt bridge (SB) and Zn^{2+}-ligand interaction distances during Hv1 F·Zn^{2+} c0 MD simulation without Zn^{2+}-His-$N_{\delta1}$ harmonic constraints.** Related to Figs. 5 and 6. **(A–L)** Calculated Zn^{2+}-ligand interaction or salt bridge distances (A, C, E, G, I, and K) and their respective frequency distributions (B, D, F, H, J, and L) are shown for selected residue pairs: A and B: ZN^{17}-$H^{2.40}$-$N_{\delta1}$ andZN^{17}-$H^{3.71}$-$N_{\delta1}$; C and D: $D^{3.50}$-R1,$D^{3.50}$-R2, and $D^{3.50}$-R3; E and F: $E^{3.47}$-R3, $E^{3.47}$-$K^{2.57}$, and $E^{3.47}$-$K^{5.46}$; G and H: $E^{5.50}$-$R^{5.51}$ and $E^{5.50}$-$K^{5.46}$; I and J: $D^{1.69}$-$K^{1.70}$; K, L: $E^{2.64}$-$R^{2.62}$. Distances are binned at 0.25-Å intervals.

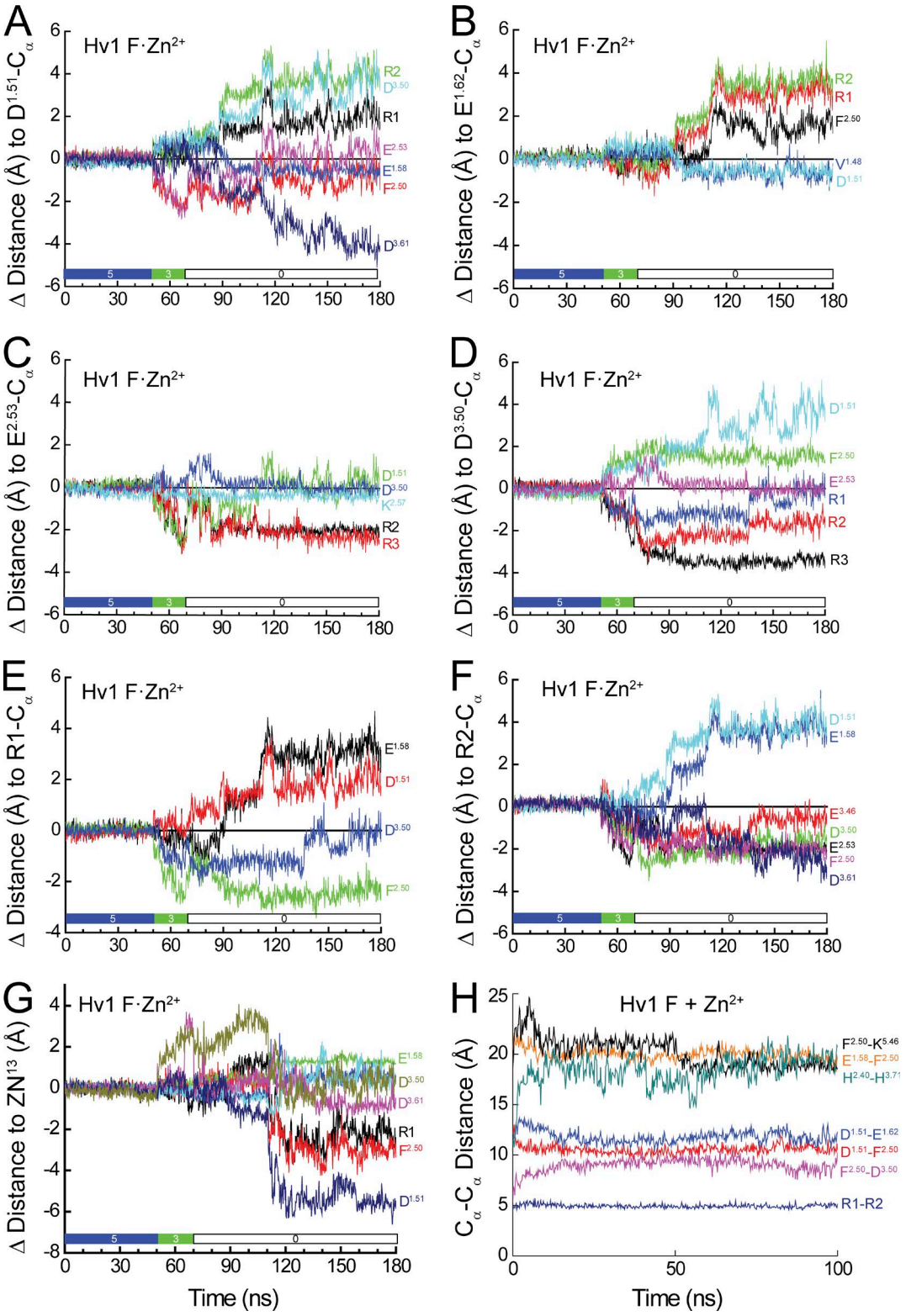

Figure S8. **Changes in C_α positions before (Hv1 F·Zn^{2+} c5) and after (Hv1 F·Zn^{2+} c0) relief of Zn^{2+}-His-$N_{\delta1}$ harmonic constraints.** Related to Figs. 5 and 6. **(A–G)** Changes in the distance between C_α atoms of $D^{1.51}$ (A), $E^{1.62}$ (B), $E^{2.53}$ (C), $D^{3.50}$ (D), R1 (E), R2 (F), or ZN^{13} (G) and the indicated residue C_α atoms during the full Hv1 F·Zn^{2+} MD trajectory with (c5, blue bar; c3, green bar) and without (c0, white bar) harmonic constraints applied to ZN^{13}-$H^{2.40}$-$N_{\delta1}$ and ZN^{13}-$H^{3.71}$-$N_{\delta1}$ bonds are shown by colored lines: (A) green, R2; cyan, $D^{3.50}$; black, R1; magenta, $E^{2.53}$; blue, $E^{1.58}$; red, $F^{2.50}$; indigo, $D^{3.61}$; (B) green, R2; red, R1; black, $F^{2.50}$; cyan, $D^{1.51}$; blue, $V^{1.48}$; (C) green, $D^{1.51}$; blue, $D^{3.50}$; cyan, $K^{2.57}$; black, R2; red, R3; (D) cyan, $D^{1.51}$; green, $F^{2.50}$; magenta, $E^{2.53}$; blue, R1; red, R2; black, R3; (E) black, $E^{1.58}$; red, $D^{1.51}$; blue, $D^{3.50}$; green, $F^{2.50}$; (F) cyan, $D^{1.51}$; blue, $E^{1.58}$; red, $E^{3.46}$; green, $D^{3.50}$; black, $E^{2.53}$; magenta, $F^{2.50}$; indigo, $D^{3.61}$; (G) green, $E^{1.58}$; olive, $D^{3.50}$; magenta, $D^{3.61}$; black, R1; red, $F^{2.50}$; indigo, $D^{1.51}$. **(H)** Distances between C_α atoms during the Hv1 F + Zn^{2+} MD simulation trajectory are indicated by lines (black, $F^{2.50}$-$K^{5.46}$; orange, $E^{1.58}$-$F^{2.50}$; teal, $H^{2.40}$-$H^{3.71}$; blue, $D^{1.51}$-$E^{1.62}$; red, $D^{1.51}$-$F^{2.50}$; magenta, $F^{2.50}$-$D^{3.50}$; indigo, R1-R2).

Table S1. **Distance restraints for the last three rounds of Hv1 model refinement**

Round	Atom 1	Atom 2	Mean bound distance	Modeller protocol
			Å	
2	H140-$N_{\delta1}$	H193-$N_{\delta1}$	Upper: 10 ± 0.1 Å	physical.xy_distance
			Lower: 6 ± 0.1 Å	
2	K157-N_{ζ}	K221-N_{ζ}	Upper: 5 ± 0.1 Å	physical.coulomb
2	D174-$O_{\delta1}$	R208-N_{H1}	Upper: 5 ± 0.1 Å	physical.coulomb
2	E171-$O_{\varepsilon1}$	R211-N_{H1}	Upper: 5 ± 0.1 Å	physical.coulomb
2	E153-$O_{\varepsilon1}$	R205-N_{H1}	Upper: 5 ± 0.1 Å	physical.coulomb
3	H140-$N_{\varepsilon2}$	H193-$N_{\varepsilon2}$	Upper: 10 ± 0.1 Å	physical.xy_distance
			Lower: 6 ± 0.1 Å	
3	K157-N_{ζ}	K221-N_{ζ}	Upper: 5 ± 0.1 Å	physical.coulomb
3	D174-$O_{\delta1}$	R208-N_{H1}	Upper: 5 ± 0.1 Å	physical.coulomb
3	E171-$O_{\varepsilon1}$	R211-N_{H1}	Upper: 5 ± 0.1 Å	physical.coulomb
3	E153-$O_{\varepsilon1}$	R208-N_{H1}	Upper: 5 ± 0.1 Å	physical.coulomb
3	E119-$O_{\varepsilon1}$	D185-$O_{\delta2}$	Upper: 15 ± 0.1 Å	physical.coulomb
3	D123-$O_{\delta1}$	D185-$O_{\delta1}$	Upper: 15 ± 0.1 Å	physical.coulomb
3	D130-$O_{\delta1}$	H193-$N_{\varepsilon2}$	Upper: 15 ± 0.1 Å	physical.coulomb
4	H140-$N_{\delta1}$	H193-$N_{\delta1}$	Upper: 3 ± 0.01 Å	physical.xy_distance
			Lower: 3 ± 0.01 Å	
4	H140-$N_{\varepsilon2}$	D185-C_{γ}	Upper: 4 ± 0.01 Å	physical.xy_distance
4	H193-$N_{\varepsilon2}$	D185-C_{γ}	Upper: 4 ± 0.01 Å	physical.xy_distance
4	H140-$N_{\delta1}$	E119-C_{γ}	Upper: 5 ± 0.01 Å	physical.xy_distance
4	H193-$N_{\delta1}$	E119-C_{γ}	Lower: 5 ± 0.01 Å	physical.xy_distance
4	E171-$O_{\varepsilon1}$	K157-N_{ζ}	Upper: 5 ± 0.01 Å	physical.coulomb

Upper and lower bound forms were used to restrain either XY distances (physical.xy_distance) or the Coulomb point–point electrostatic potential (physical.coulomb) between defined atoms (Sali and Blundell, 1993; Fiser et al., 2000; Marti-Renom et al., 2000; Webb and Sali, 2014; https://salilab.org/modeller/9.16/manual.pdf). The upper and lower bound restraints are presented as mean ± SD. Atom types are defined by the CHARMM36 force field (MacKerell et al., 1998, 2004; Best et al., 2012).

Table S2. **Mean C_{α} – C_{α} distances in selected Hv1 F MD trajectories**

Atom 1	Atom 2	Location	C_{α} RMSD Hv1F + Zn^{2+} [a]	C_{α} RMSD Hv1F·Zn^{2+} (c5) [b]	C_{α} RMSD Hv1F·Zn^{2+} (c0) [c]	C_{α} RMSD Hv1F + Na^{+} [d]
			Å	*Å*	*Å*	*Å*
R208/$R^{4.50}$	F150/$F^{2.50}$	S4-S2	14.20 ± 0.67	14.14 ± 0.17	12.12 ± 0.37	13.16 ± 0.67
E119/$E^{1.58}$	D185/$D^{3.61}$	S1-S3	12.85 ± 0.79	11.68 ± 0.18	11.99 ± 0.70	13.34 ± 1.48
E153/$E^{2.53}$	R208/$R^{4.50}$	S2-S4	15.36 ± 0.95	15.29 ± 0.22	13.37 ± 0.45	14.15 ± 0.88
D174/$D^{3.50}$	R205/$R^{4.47}$	S3-S4	8.80 ± 0.45	8.02 ± 0.31	9.06 ± 0.44	9.66 ± 0.35

Distances between C_{α} atoms of the indicated residues are measured every 10th frame of each MD simulation (i.e., every 0.2 ns) using and the mean ± SD values are reported.
[a]100 ns Hv1F + Zn^{2+} MD trajectory (Fig. 5 E).
[b]Initial 50 ns of 180 ns Hv1F·Zn^{2+} MD trajectory (with 5 kcal/mol harmonic constraint between $H^{2.40}$-$N_{\delta1}$ and $H^{3.71}$-$N_{\delta1}$ applied; Fig. 5 G).
[c]Final 110 ns of 180 ns Hv1F·Zn^{2+} MD trajectory (after relief of harmonic constraints between $H^{2.40}$-$N_{\delta1}$ and $H^{3.71}$-$N_{\delta1}$; Fig. 5 G).
[d]60 ns Hv1F·Na+ MD trajectory (Fig. S5).

Table S3. **RMSD calculations for selected Hv1 F MD trajectories**

Atom 1	Atom 2	Location	C_α RMSD Hv1F + Zn^{2+} [a]	C_α RMSD Hv1F·Zn^{2+} (c5) [b]	C_α RMSD Hv1F·Zn^{2+} (c0) [c]	Δ C_α RMSD Hv1F·Zn^{2+} (c0 – c5) [b,c]	C_α RMSD Hv1F + Na^+ [d]
			Å	*Å*	*Å*	*Å*	*Å*
D112/$D^{1.51}$	F150/$F^{2.50}$	S1-S2	0.43	0.18	0.62	0.44	0.62
E119/$E^{1.58}$	F150/$F^{2.50}$	S1-S2	0.53	0.22	0.80	0.58	1.12
E153/$E^{2.53}$	F150/$F^{2.50}$	S2-S2	0.27	0.13	0.20	0.07	0.22
D174/$D^{3.50}$	F150/$F^{2.50}$	S3-S2	0.64	0.22	0.30	0.08	1.50
R205/$R^{4.47}$	F150/$F^{2.50}$	S4-S2	0.60	0.22	0.62	0.4	0.64
R208/$R^{4.50}$	F150/$F^{2.50}$	S4-S2	0.67	0.16	2.41	2.25	0.67
K221/$K^{5.46}$	F150/$F^{2.50}$	L5-S2	0.77	0.22	2.97	2.75	0.72
E225/$E^{5.50}$	F150/$F^{2.50}$	L5-S2	0.82	0.17	4.48	4.31	0.93
ZN^{2}	F150/$F^{2.50}$	Zn^{2+}-S2	0.96[b]	0.17	2.37	2.20	ND
ZN^{13}	F150/$F^{2.50}$	Zn^{2+}-S2	2.08[d]	0.23	1.61	1.38	ND
SOD^{3}	F150/$F^{2.50}$	Na^+-S2	ND	ND	ND	ND	5.60[c]
SOD^{6}	F150/$F^{2.50}$	Na^+-S2	ND	ND	ND	ND	8.06[c]
D174/$D^{3.50}$	K157/$K^{2.57}$	S3-S2	0.65	0.24	1.96	1.72	0.74
E119/$E^{1.58}$	H140/$H^{2.40}$	S2-S2	0.64	0.16	1.12	0.96	0.62
D185/$D^{3.61}$	H140/$H^{2.40}$	S3-S2	1.06	0.13	1.98	1.85	1.96
E119/$E^{1.58}$	H193/$H^{3.71}$	S1-S3L	1.15	0.17	1.06	0.89	1.47
D185/$D^{3.61}$	H193/$H^{3.71}$	S3-S3L	1.39	0.17	1.13	0.96	1.65
H140/$H^{2.40}$	H193/$H^{3.71}$	S2-S3L	1.50	0.11	0.76	0.65	2.93
D112/$D^{1.51}$	R205/$R^{4.47}$	S1-S4	0.43	0.24	0.75	0.51	0.37
E119/$E^{1.58}$	R205/$R^{4.47}$	S1-S4	0.54	0.29	1.50	1.21	0.55
E153/$E^{2.53}$	R205/$R^{4.47}$	S2-S4	0.83	0.24	0.52	0.28	0.78
E153/$E^{2.53}$	R208/$R^{4.50}$	S2-S4	0.94	0.22	0.45	0.23	0.87
E171/$E^{3.47}$	R208/$R^{4.50}$	S3-S4	1.16	0.16	1.25	1.09	1.00
E171/$E^{3.47}$	R211/$R^{4.53}$	S3-S4	1.06	0.23	0.48	0.25	1.56
D174/$D^{3.50}$	R205/$R^{4.47}$	S3-S4	0.45	0.15	0.61	0.46	0.35
D174/$D^{3.50}$	R208/$R^{4.50}$	S3-S4	0.32	0.19	0.46	0.27	0.79
R205/$R^{4.47}$	R208/$R^{4.50}$	S4-S4	0.18	0.14	0.18	0.04	0.17

RMSDs are calculated from the distance in positions of indicated atoms at every 10th frame of each MD simulation (i.e., every 0.5 ns) using the function $RMSD = \sqrt{mean(D^2)}$, where $D^2 = (X_{frame} - X_{mean})^2$ and X_{frame} is the distance between atom1 and atom 2 at each time point and X_{mean} is the mean distance between atom1 and atom 2 over the indicated trajectory time.

[a]100 ns Hv1F + Zn^{2+} MD trajectory (Fig. 5 E).

[b]Initial 50 ns of 180 ns Hv1F·Zn^{2+} MD trajectory (with 5 kcal/mol harmonic constraint between $H^{2.40}$-$N_{\delta1}$ and $H^{3.71}$-$N_{\delta1}$ applied; Fig. 5 G).

[c]Final 110 ns of 180 ns Hv1F·Zn^{2+} MD trajectory (after relief of harmonic constraints between $H^{2.40}$-$N_{\delta1}$ and $H^{3.71}$-$N_{\delta1}$; Fig. 5 G).

[d]60 ns Hv1F·Na^+ MD trajectory (Fig. S5).

Table S4. **Salt bridges in selected Hv1 F MD trajectories**

Residue 1	Residue 2	Salt bridge distance Hv1F + Zn^{2+} [a]	Salt bridge distance Hv1F·Zn^{2+} (c5) [b]	Salt bridge distance Hv1F·Zn^{2+} (c0) [c]	Salt bridge distance Hv1F + Na^{+} [d]
		Å	*Å*	*Å*	*Å*
D112/$D^{1.51}$	R205/$R^{4.47}$	4.21	3.16	4.25	3.29
D112/$D^{1.51}$	R208/$R^{4.50}$	–	4.12	9.77	4.73
D112/$D^{1.51}$	R211/$R^{4.53}$	–	10.00	12.86	–
E119/$E^{1.58}$	R205/$R^{4.47}$	–	–	–	9.80
E153/$E^{2.53}$	R205/$R^{4.47}$	9.91	–	–	–
E153/$E^{2.53}$	K157/$K^{2.57}$	4.57	2.93	–	3.88
E153/$E^{2.53}$	R208/$R^{4.50}$	9.12	9.08	–	6.11
E153/$E^{2.53}$	R211/$R^{4.53}$	–	–	–	9.27
E153/$E^{2.53}$	K221/$K^{5.46}$	–	8.35	–	10.86
E171/$E^{3.47}$	K157/$K^{2.57}$	4.56	3.32	–	2.92
E171/$E^{3.47}$	R208/$R^{4.50}$	5.47	8.72	–	7.73
E171/$E^{3.47}$	R205/$R^{4.53}$	9.40	8.79	–	6.97
E171/$E^{3.47}$	K221/$K^{5.46}$	9.22	6.21	–	9.30
D174/$D^{3.50}$	K157/$K^{2.57}$	6.77	8.07	–	7.43
D174/$D^{3.50}$	R205/$R^{4.47}$	7.51	4.30	6.66	7.33
D174/$D^{3.50}$	R208/$R^{4.50}$	3.36	3.39	4.30	4.94
D174/$D^{3.50}$	R205/$R^{4.53}$	–	7.84	–	5.48
E225/$E^{5.50}$	K157/$K^{2.57}$	4.57	8.08	–	–
E225/$E^{5.50}$	K221/$K^{5.46}$	9.56	3.47	–	3.14

Mean salt bridge (7 Å distance cutoff between oxygen and nitrogen atoms) distances and fractional occupancy of H-bonds between listed residue pairs are calculated for every 10th frame of each MD simulation (i.e., every 0.2 ns) using plugins in VMD 1.9.3 (see Materials and methods).
[a]100 ns Hv1F + Zn^{2+} MD trajectory (Fig. 5 E).
[b]Initial 50 ns of 180 ns Hv1F·Zn^{2+} MD trajectory (with 5 kcal/mol harmonic constraint between $H^{2.40}$-$N_{\delta 1}$ and $H^{3.71}$-$N_{\delta 1}$ applied; Fig. 5 H).
[c]Final 110 ns of 180 ns Hv1F·Zn^{2+} MD trajectory (after relief of harmonic constraints between $H^{2.40}$-$N_{\delta 1}$ and $H^{3.71}$-$N_{\delta 1}$; Fig. 5 H).
[d]60 ns Hv1F·Na^{+} MD trajectory.

Table S5. **Occupancy of selected H-bonds in Hv1 F MD trajectories**

Residue 1	Residue 2	HBs Hv1F + Zn^{2+} [a]	HBs Hv1F·Zn^{2+} (c5) [b]	HBs Hv1F·Zn^{2+} (c0) [c]	HBs Hv1F + Na^{+} [d]
		%	%	%	%
D112/D1.51	R205/R4.47	46.31	77.69	50.91	–
D112/D1.51	R208/R4.50	–	–	7.09	27.62
E153/E2.53	R205/R4.47	–	–	–	–
E153/E2.53	K157/K2.57	10.98	32.67	5.82	31.61
E153/E2.53	R208/R4.50	–	–	–	7.15
E153/E2.53	R211/R4.53	–	–	120.18	–
E171/E3.47	K157/K2.57	28.34	60.56	58.73	54.21
E171/E3.47	R208/R4.50	39.32	–	–	2.33
E171/E3.47	R211/R4.53	–	–	0.18	–
E171/E3.47	K221/K5.46	–	–	–	–
D174/D3.50	K157/K2.57	–	–	–	–
D174/D3.50	R205/R4.47	–	56.18	–	17.14
D174/D3.50	R208/R4.50	134.53	–	20.36	19.13
D174/D3.50	R211/R4.53	–	–	122.18	36.44
D174/D3.61	H140/H2.40	0.6	–	–	–
E225/E5.50	K157/K2.57	52.3	–	–	–
E225/E5.50	K221/K5.46	–	–	34.91	54.24

Fractional occupancy of H-bonds (HBs) within a 3.0 Å distance and 20° angle cutoff between donor and acceptor atoms of the listed residues are calculated for every 10th frame of each MD simulation (i.e., every 0.2 ns) using the plugin in VMD 1.9.3 (see Materials and methods).
[a]100 ns Hv1F + Zn^{2+} MD trajectory (Fig. 5 E).
[b]Initial 50 ns of 180 ns Hv1F·Zn^{2+} MD trajectory (with 5 kcal/mol harmonic constraint between $H^{2.40}$-$N_{\delta1}$ and $H^{3.71}$-$N_{\delta1}$ applied; Fig. 5 H).
[c]Final 110 ns of 180 ns Hv1F·Zn^{2+} MD trajectory (after relief of harmonic constraints between $H^{2.40}$-$N_{\delta1}$ and $H^{3.71}$-$N_{\delta1}$; Fig. 5 H).
[d]60 ns Hv1F·Na^{+} MD trajectory.

References

Best, R.B., X. Zhu, J. Shim, P.E. Lopes, J. Mittal, M. Feig, and A.D. Mackerell Jr. 2012. Optimization of the additive CHARMM all-atom protein force field targeting improved sampling of the backbone φ, ψ and side-chain χ(1) and χ(2) dihedral angles. *J. Chem. Theory Comput.* 8:3257–3273. https://doi.org/10.1021/ct300400x

Fiser, A., R.K. Do, and A. Sali. 2000. Modeling of loops in protein structures. *Protein Sci.* 9:1753–1773. https://doi.org/10.1110/ps.9.9.1753

MacKerell, A.D., D. Bashford, M. Bellott, R.L. Dunbrack, J.D. Evanseck, M.J. Field, S. Fischer, J. Gao, H. Guo, S. Ha, et al. 1998. All-atom empirical potential for molecular modeling and dynamics studies of proteins. *J. Phys. Chem. B.* 102:3586–3616. https://doi.org/10.1021/jp973084f

MacKerell, A.D. Jr., M. Feig, and C.L. Brooks III. 2004. Improved treatment of the protein backbone in empirical force fields. *J. Am. Chem. Soc.* 126:698–699. https://doi.org/10.1021/ja036959e

Martí-Renom, M.A., A.C. Stuart, A. Fiser, R. Sánchez, F. Melo, and A. Sali. 2000. Comparative protein structure modeling of genes and genomes. *Annu. Rev. Biophys. Biomol. Struct.* 29:291–325. https://doi.org/10.1146/annurev.biophys.29.1.291

Sali, A., and T.L. Blundell. 1993. Comparative protein modelling by satisfaction of spatial restraints. *J. Mol. Biol.* 234:779–815. https://doi.org/10.1006/jmbi.1993.1626

Webb, B., and A. Sali. 2014. Comparative Protein Structure Modeling Using MODELLER. *Curr. Protoc. Bioinformatics*. 47:5.6.1–5.6.32. https://doi.org/10.1002/0471250953.bi0506s47